IET Journals
The Institution of Engineering and Technology

# Hybrid Battery-Ultracapacitor Storage System Sizing for Renewable Energy Network Integration

ISSN 1751-8644
doi: 0000000000
www.ietdl.org

*Jose M. Gonzalez-Gonzalez*[1*], *Sebastian Martin*[1], *Pablo Lopez*[1], *Jose A. Aguado*[1]

[1] *Department of Electrical Engineering, Universidad de Málaga, C/ Doctor Ortiz Ramos s/n, 29071 Málaga, Spain*
[*] *E-mail: josemanuelgonzalez@uma.es*

**Abstract:** Wind and Solar photovoltaic power plants outputs are usually highly variable due to gusts of wind and sharp sun irradiance level variations caused by cloud shadding effects. These effects negatively impact system security, specially in weak power networks. On the other hand, due to recent technological progress and cost reductions, electrical energy storage systems are an attractive alternative that can be easily integrated into non-dispatchable power plants to compensate for those power output fluctuations. This paper proposes a methodology for optimal sizing of a Hybrid (lithium-ion battery and ultracapacitor) Energy Storage System for renewable energy network integration. Special attention is paid to the battery cycling degradation process. It is shown that battery aging due to cycling is a major driver for optimal sizing. The resulting sizing problem is posed as a Non-Linear Programming problem. Finally, real and illustrative case studies are presented for both, Wind and PV power plants integrating a Hybrid Energy Storage System. Results are reported by comparing different energy storage system configurations.

## Notation

### *Indices and sets*

| | |
|---|---|
| $n, N$ | Index and set for cycles in the load profile, $n \in N$. |
| $t, T$ | Index and set for periods of time, $t \in T$. |

### *Parameters*

| | |
|---|---|
| $C^b$ | Battery cost per kWh, [$/kWh]. |
| $C^{inv}$ | Inverter cost per kW, [$/kW]. |
| $C^u$ | Ultracapacitor cost per kWh, [$/kWh]. |
| $CL^b$ | Battery calendar life, [h]. |
| $CL^{inv}$ | Inverter calendar life, [h]. |
| $CL^u$ | Ultracapacitor calendar life, [h]. |
| $Crate^{b,max}$ | Maximum power flow by the battery, [p.u.]. |
| $Crate^{u,max}$ | Maximum power flow for the ultracapacitor, [p.u.]. |
| $ESG_n$ | Energy transferred from the storage system to the grid in period $n$, [kWh]. |
| $EGS_n$ | Energy transferred from the grid to the storage system in period $n$, [kWh]. |
| $P^{max}$ | Maximum power in the storage system load profile, [kW]. |
| $SOC_0^b$ | Initial battery state of charge, [p.u.]. |
| $\underline{SOC}^b$ | Minimum battery state of charge, [p.u.]. |
| $\underline{SOC}^u$ | Minimum ultracapacitor state of charge, [p.u.]. |
| $T^{prof}$ | Profile total duration, [h] |
| $\alpha/\beta/\gamma$ | Coefficients of the battery degradation curve. |
| $\Delta T_n$ | Lasting of cycle $n$, [h]. |
| $\eta^{b,c}$ | Battery charging efficiency, [p.u.]. |
| $\eta^{b,d}$ | Battery discharging efficiency, [p.u.]. |
| $\eta^{inv}$ | Inverter efficiency, [p.u.]. |
| $\eta^{u,c}$ | Ultracapacitor charging efficiency, [p.u.]. |
| $\eta^{u,d}$ | Ultracapacitor discharging efficiency, [p.u.]. |

### *Positive variables*

| | |
|---|---|
| $e_n^b$ | Battery charging or discharging energy for cycle $n$, [kWh]. |
| $e_{rated}^b$ | Battery energy storage rated capacity, [kWh]. |
| $e_n^{b,c}$ | Battery charging energy for cycle $n$, [kWh]. |
| $e_n^{b,d}$ | Battery discharging energy for cycle $n$, [kWh]. |
| $e_{rated}^u$ | Ultracapacitor energy rated capacity, [kWh]. |
| $e_n^{u,c}$ | Ultracapacitor charging energy for cycle $n$, [kW]. |
| $e_n^{u,d}$ | Ultracapacitor discharging energy for cycle $n$, [kW]. |
| $fol^b$ | Total battery life consumed, [p.u.]. |
| $fol_n^b$ | Fraction of battery life consumed for cycle $n$, [p.u.]. |
| $fol_n^{b,CL}$ | Fraction of battery life consumed due to calendar for cycle $n$, [p.u.]. |
| $fol_n^{b,OP}$ | Fraction of battery life consumed due to operation for cycle $n$, [p.u.]. |
| $p^{inv}$ | Inverter rated power, [kW]. |
| $soc_n^b$ | Accumulated energy in the battery at cycle $n$, [kWh]. |
| $soc_n^u$ | Accumulated energy in the ultracapacitor at cycle $n$, [kWh]. |

## 1 Introduction

Wind and solar PV plants are essential to reduce the greenhouse emissions and the dependence of fossil fuels. The implementation of these technologies is occurring at a very high rate and is expected that they will produce 50% of the world electricity generation by 2050 [1]. However, these energy sources are intermittent by nature, their generation is non dispatchable and they could negatively impact grid stability [2], [3]. The reliability of the electricity supply is a mandatory requirement in recent grid codes, especially for isolated power systems with high renewable energy shares. Puerto Rico's Grid Code [4] is an example in which PV power output fluctuations are restricted to 10% per minute of the plant's rated power. This constraint is also recommended by National Renewable Energy Laboratory (NREL) [5] and the german Transmission System Operator [6]. Other similar conditions are applied for instance in Ireland, where EirGrid (Ireland grid operator) limits positive ramps up to 30 MW/minute. Additionally, in Hawai, where the Hawaiian Electric Company (HECO) limits the ramps to +/-2 MW per minute during all times. In addition to one-minute ramp rate restrictions, other grid operators include instantaneous restrictions in their network codes, such as HECO, which includes a ramp rate limit of 1 MW per 2 seconds.

Electrical Energy Storage Systems (ESS) are regarded as one of the key technologies to face the challenges posed by renewable energy sources. They have evolved as a fast pace over the last years, specially in what is related to battery technologies, achieving an excellent technical performance while at the same time reducing prices [7]. For instance, lithium-ion battery cost for Electric Vehicle (EV) applications is under 200 $/kWh nowadays, and it is expected to be reduced in the future to 100 $/kWh by 2030 [8, 9]. Nevertheless, these costs are not applied to stationary applications because they require additional components and their function is usually more stressful for the battery chemistry. The cost of batteries for stationary applications is currently above 500 $/kWh and forecasts indicate that 200$/kWh will be reached by 2030 [8, 10, 11]. Stationary applications include, among others, load peak shaving and power smoothing [12, 13], voltage regulation [14], frequency regulation [15], and increment of stability in isolated systems [16].

Battery storage systems are in the spotlight because some of their characteristics, such as energy density, power density or scalability. And they are ideal for some renewable generation applications. But there are also other alternative storage technologies with different capabilities and important applications. Probably the most known is the pumped storage. It is ideal to balance demand and generation in medium/large-periods. Usually it is used as a large-scale energy storage, and requires high initial investments. Also for large-scale applications we found the Compressed Air Energy Storage (CAES). However, these technologies are not suitable to respond to short-period (fast response) perturbations. On the other hand, flywheels, Superconducting Magnetic Energy Storage (SMES) and ultracapacitors are more appropriate for fast response applications.

A Hybrid Energy Storage System (HESS) combine the characteristics and benefits of two different types of storage technologies [17], enhancing the global features of the system, in particular, reducing the operating costs and increasing the lifetime and efficiency [18]. In systems with high renewable penetration, especially isolated systems, the use of a HESS (lithium-ion batteries and ultracapacitors) is advised, because it allows to reduce the output power fluctuations by combining the energy density of batteries and the power density of ultracapacitors [17]. Although ultracapacitors are not suitable to store energy in a high quantity and/or in the long term due to their high cost per kWh and their self-discharge rate [19], they provide high power delivery. In addition to reducing output power fluctuations, it can also improve the resilience to faults of the generation system, since the storage is able to continue providing energy during a short period.

Sizing a HESS is not a trivial task and has been the focus of attention of some researchers. One of the most known applications for HESSs are the Electric Vehicles (EV), because the HESSs provide high power, required for acceleration and regenerative braking, and also storage capability for EV distance range. An illustrative analysis of optimal sizing for a city bus can be found in [20], where the authors compare batteries, ultracapacitors and HESS solutions. Another sizing algorithm for fuel cell hybrid EVs is described in [21], ], whose authors propose a multi-objective optimization problem. The optimization seeks to ensure an optimal power sharing in order to increase the energy efficiency and minimize the storage system weight and the hydrogen consumption. The problem has been formulated for a frequency-separation-based energy management, which decomposes the total load power into three different load profiles according to the frequency of the variations: the low frequency profile is used for the fuel cell sizing, the medium frequency profile for the battery sizing and the high frequency profile for the ultracapacitor sizing.

Focusing on stationary applications, strategies to deal with the variability of PV plants can be found in the literature. For instance, a power smoothing strategy for a 1 MW PV plant is presented in [22], which allows to reduce the fluctuating output power using a HESS composed of vanadium-redox batteries and a supercapacitor bank, in order to increase the global system efficiency. An strategy for ramp-rate control is also presented in [23], in which the authors describe a HESS for a PV plant, simulating its operation and calculating the net present cost over project life. This study concludes that the ramp-rate constraint has a significant impact on the profitability of the system. The authors of [24] propose a multi-objective sizing methodology for large-scale photovoltaic power generation system, in which the algorithm selects the storage system by comparing different combinations and considering the effects of multiple weather conditions.

Stationary applications not only include PV generation but also wind generation, whose high variability makes hybrid systems ideal to solve this inconvenient. A typical application is to smooth wind power fluctuations. An example can be found in [25], where is described a HESS sizing method that considers only the power ramp rate. HESSs are also appropriate for grid applications. An example of a HESS providing ancillary services is the fast response to frequency deviations in systems with high renewable penetration, such as in [16] and [26], where HESS sizing algorithms are described.

Most of these studies do not include the degradation of the HESS components or it has been considered with a low accuracy. On one hand, ultracapacitors have low cycling degradation and their lifespan is usually defined by its calendar life. On the other hand, how batteries are operated has a great influence in their lifespan and should be taken into account when sizing them.

Battery degradation has been studied by many authors. For instance, in [27], a semi-empirical degradation model for lithium-ion battery is proposed. It explains that the degradation depends on four parameters of the operating cycles: duration, State of Charge (SoC), Depth of Discharge (DoD) and temperature. The results are compared with the data provided by the manufacturers. Another battery degradation model is proposed in [28], in which the authors considerate the cycle current and DoD, based on the electrochemical mechanism of capacity fade. Battery degradation has a real impact on the life and profitability of ESS as demonstrated in [29], which analyzes the operation of Vehicle-to-Grid (V2G) systems and concludes that considering battery degradation in the operation would provide between 2-5% additional benefit compared to smart charging. The impact of the battery degradation has not been translated to the sizing of the HESS and the literature does not show a wide variety of sizing algorithms for battery storage considering degradation by operation. An example is the algorithm presented in [30], in which the authors propose a battery sizing algorithm using the cycles-to-fail curves provided by manufacturers, which depends on two parameters: cycles DoD and C-rate. An example of this curve can be found in [31]. The authors of [32] also present a genetic algorithm to size a HESS for electric vehicles considering battery degradation. This algorithm provides multiple sizing solutions with their relationship between the weight and the cycle life of the battery. The calculation is based on a detailed degradation model, but this model requires a high computational cost and the use of parameters whose values are not usually provided by manufacturers. Although the algorithm provides multiple solutions, they do not consider capital and operational expenditures, and the selection of one particular solution is left to the user. Another sizing algorithm for hybrid energy storage system is presented in [33] for wind power. The optimization problem uses a hybrid particle swarm optimization-genetic algorithm to obtain the optimal solution. The authors model the degradation of the battery, but they do not consider the influence of the C-rate in the model.

The control strategy decides how to operate the hybrid energy storage system. Although the analysis of the different control strategies is not in the scope of this paper, it affects to the solution of the sizing problem. A strategy to reduce the charging/discharging battery stress has been selected. The strategy is based on reducing the C-rate and DoD of the battery charging cycles. Several authors proposed this control strategy, such as in [34–36].

The main contribution of this paper consists of the definition of a HESS sizing methodology compatible with multiple applications which includes the degradation of their components. In order to achieve this objective, a HESS detailed model is implemented, including the battery, the ultracapacitors and the power converters. The HESS sizing and operation is posed as a non-linear optimization problem.

This paper is organized as follows. A description of the HESS chosen topology is presented in Section 2. Sizing methodology is explained in Section 3. Equations and constrains are formulated

in Section 4. Two application cases, PV and wind, are studied in Section 5. Conclusions in Section 6 close the paper.

## 2 Electric Energy Storage and Ultracapacitor System Architecture

As discussed in the previous section, the aim of this paper is to optimize the size of a HESS composed of batteries and ultracapacitors. As these elements can be combined following different topologies [37], in this section the topology selected here is described.

Although it is possible to install an inverter for each element of the hybrid system, the higher initial investment required makes usual common inverter is used for both. In systems with shared inverters, the differences between topologies are in the way of connecting each storage technology to the DC bus of the inverter, so that it is possible to classify them into two main types: actives and passives.

Passive systems have the simplest topology, since both elements are connected directly to the DC bus so that the ultracapacitor acts naturally smoothing the power peaks received by the battery and reducing the stress it suffers. However, this type of hybrid system does not allow to control individually each storage element and they, specially ultracapacitors, cannot take advantage of all their storage and power capacity. The active hybrid systems do not have this drawback thanks to the use of DC-DC converters, which allow to isolate the voltages of the storage elements and control them individually. In this case, the connection possibilities are reduced to the use of a DC-DC converter for each element, one only for the battery or one exclusive for the ultracapacitor.

For the development of this paper, the last option has been selected, since it simplifies the control over two DC-DC converters and reduces the investment. Moreover, this topology improves the efficiency because most of the energy is managed by the battery, which is connected to the DC bus without a converter. An scheme of this topology is presented in Fig. 1.

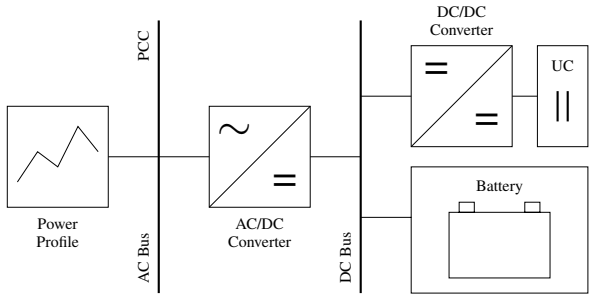


**Fig. 1**: Hybrid storage topology.

The proposed architecture is connected in parallel to the generation system since it has its own inverter. By not sharing components, the capital cost of the storage increases, but in return, the resilience to faults and the compatibility with other systems are improved.

## 3 Methodology

Given a load profile to be faced by a HESS made up of battery and ultracapacitor, the problem to size the HESS taking into account the battery ageing leads to a non-linear optimization problem. The HESS load profile is a sequence of cycles, where each cycle is defined by its energy (charging or discharging) and its duration. Battery ageing is due to operation and the time, calendar life. The link between battery ageing and its operation is a non-linear function that for each cycle $n$ has the form $(\frac{1}{2\gamma}) \cdot (C-rate_n)^{\alpha} \cdot (dod_n)^{\beta}$, where $C-rate_n = \frac{e^b_n}{e^b_{rated} \cdot \Delta T_n}$ is the battery C-rate at cycle $n$, and $dod_n = \frac{e^b_n}{e^b_{rated}}$ is the battery Depth of Discharge for cycle $n$. The battery ageing for the whole load profile is accounted by the variable $fol^b = \sum_{n=1}^{N} fol_n$. Both converters and ultracapacitors ageing is computed using their calendar life. Although the manufacturers also provide the number of cycles to the failure of the ultracapacitors, this value is very high [38] that their degradation by operation has no practical effect on the results.

Here it is assumed there is no power interchange between battery and ultracapacitor, therefore for each period of time the load profile is partitioned between the battery and the ultracapacitor. This operation is performed according to an optimization problem which decides the amount of energy that flows from or to the battery and the ultracapacitor. Thus, the sizing and operation problem consists in determining the size of each device, battery and ultracapacitor, and the part of the load profile faced by each one.

The battery ageing model could be included in the optimization problem and solved using commercial software (off the shelf) if it is posed as a smooth derivable function on the decision variables in the problem. For this purpose, the ageing model is adapted to be included in the optimization problem, resulting a non-linear optimization problem. The adaptation is the key point in the proposed methodology, it keeps the accuracy of the ageing model and consists of the steps that follows:

1. As the battery ageing depends on the $C-rate_n$ and $dod_n$ at each load cycle $n$, we use directly the load cycles as input data in the optimization problem instead of the representation based on time. Thus, the load profile faced by the HESS is a sequence of cycles where each cycle is defined by its energy and duration.
2. The input data for each cycle in the load profile are the cycle energy and the cycle duration. The energy of each cycle is partitioned between the battery and the ultracapacitor by the optimization problem, so the sum of each part is the total energy in the load cycle.
3. $dod_n$ is directly computed from the energy assigned to battery at cycle $n$ and the battery size. For the calculation of $C-rate_n$, its value is assumed as the average power value on the cycle duration. Thus it can be computed using the energy assigned to the battery cycle, the cycle duration and the battery size, resulting a continuous and derivable function of the variables in the problem.
4. In order to avoid infeasibilities because of the maximum $C-rate$ in the load profile over time, an additional linear constraint is added to the problem. This linear constraint sets the combined contributions of the battery and ultracapacitor to the C-rate are greater or equal to the maximum power (in absolute value) in the ESS load profile over time.

Fig. 2a and 2b depict an example of the change in the initial power profile. Energy and length are calculated in each charging and discharging cycle.

## 4 Formulation

The algorithm proposed in this paper takes as input data an energy profile to by faced by the ESS. The ESS has to comply with this operating profile at all times, respecting the technical constraints and minimizing the operating costs, taking into account both capital expenditures and battery degradation.

The following subsections detail the constraints associated with each element of the HESS, as well as the objective function that considers the operating costs.

### *4.1 Energy balance*

In order to facilitate the formulation of the problem, the operation profile is decomposed into energy ($EGS_n$) that flows from the grid to the ESS, and from the ESS to the grid ($ESG_n$), being only one of them greater than zero while the other, or both, remain at zero in each cycle $n$. The first parameter, $EGS_n$, indicates the total charging energy of the battery ($e^{b,c}_n$) and the ultracapacitor ($e^{u,c}_n$) in each cycle $n$. Its balance is defined by eq. (1). Similarly, $ESG_n$ represents the sum of the discharging energy of the battery ($e^{b,d}_n$) and the ultracapacitor ($e^{u,d}_n$) in each cycle, being the energy balance defined by (2).

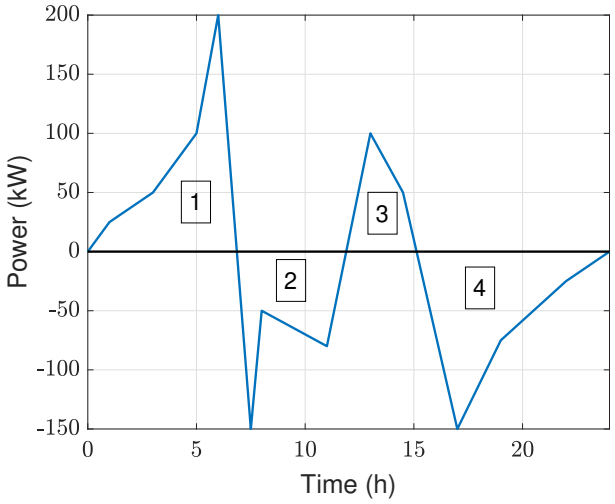


(a)

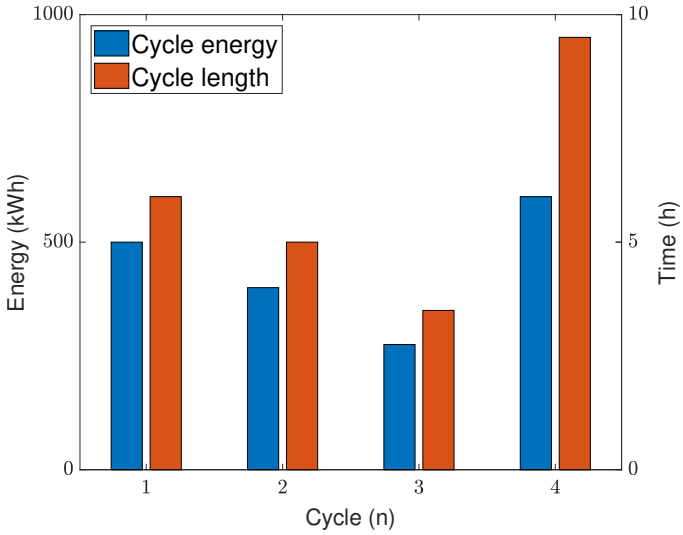


(b)

**Fig. 2**: Time index to cycle index example.

$$EGS_n = e_n^{b,c} + e_n^{u,c}; \quad \forall n \in N \tag{1}$$

$$ESG_n = e_n^{b,d} + e_n^{u,d}; \quad \forall n \in N \tag{2}$$

### 4.2 Inverter

The inverter connects the HESS with the grid, so its rated power is established by the maximum charging and discharging power of the operation profile. This constraint is defined by equation (3). Moreover, inverters work with a charging and discharging efficiency which affects the energy that flows from the grid to the storage system and vice versa. However, inverter performance is included in the battery and ultracapacitor state of charge equations presented in following subsections.

$$p^{inv} \geq P^{max}; \tag{3}$$

### 4.3 Battery

To compute the battery state of charge, it is necessary to perform an energy balance in each cycle which depends on the energy stored in the previous cycle and the charging or discharging energy of the current cycle. The energy balance must include the efficiency for both the battery and the inverter, which affects differently whether it is charging or discharging. The state of charge is defined by the following equation:

$$soc_n^b = soc_{n-1}^b + (\eta^{inv} \cdot \eta^{b,c} \cdot e_n^{b,c} - \frac{e_n^{b,d}}{\eta^{inv} \cdot \eta^{b,d}}); \quad \forall n \in N \tag{4}$$

$$soc_0^b = SOC_0^b \tag{5}$$

The battery state of charge value must move within a set range. The upper limit (6) determines the maximum amount of energy that battery can store and its value corresponds to the battery energy rated capacity, while the lower limit (7) depends on the selected battery technology and meets technical operation limits and to avoid very low states of charge which degrade it excessively.

$$e_{rated}^b \geq soc_n^b; \quad \forall n \in N \tag{6}$$

$$\underline{SOC}^b \cdot e_{rated}^b \leq soc_n^b; \quad \forall n \in N \tag{7}$$

Other constraints are related to the battery C-rate, that depends on the battery technology. The constraints for charging and discharging are defined by the equations that follow:

$$\frac{e_n^{b,c}}{\Delta T_n} \leq Crate^{b,max} \cdot e_{rated}^b; \quad \forall n \in N \tag{8}$$

$$\frac{e_n^{b,d}}{\Delta T_n} \leq Crate^{b,max} \cdot e_{rated}^b; \quad \forall n \in N \tag{9}$$

As previously mentioned, battery aging is fundamentally due to two factors: calendar life and operation. The first of these factors refers to wear due to the passage of time and is not influenced by the use of the battery, so the calculation of this degradation in each cycle depends exclusively on the cycle duration:

$$fol_n^{b,CL} = \frac{\Delta T_n}{CL^b}; \quad \forall n \in N \tag{10}$$

The calculation of the aging by operation depends on several factors such as the $dod$ of the cycle, the average $C-rate$ and the technology of the battery. The calculation method used for this type of degradation is based on the information provided by the manufacturers with the cycles-to-failure curves, whose value depends on the $dod$ and $C-rate$. Fraction of life is computed for charging and discharging individually and not for a whole cycle as usually in order to avoid the asymmetries between both profiles. The term to the power of $\alpha$ refers to $C-rate$, while the term to the power of $\beta$ corresponds to $dod$.

$$e_n^b = e_n^{b,c} + e_n^{b,d}; \quad \forall n \in N \tag{11}$$

$$fol_n^{b,OP} = \frac{\left(\frac{e_n^b}{e_{rated}^b \cdot \Delta T_n}\right)^{\alpha} \cdot \left(\frac{e_n^b}{e_{rated}^b}\right)^{\beta}}{2 \cdot \gamma}; \quad \forall n \in N \tag{12}$$

The fraction of life consumed in each cycle ($fol_n^b$) is calculated as the highest value between fraction of life consumed per lifetime and per operation:

$$fol_n^b = \max\,(fol_n^{b,CL}, fol_n^{b,OP}); \quad \forall n \in N \tag{13}$$

Finally, the fraction of total life of the battery ($fol^b$) consumed for the given profile is the sum of the fraction consumed in all the cycles that make up the profile:

$$fol^b = \sum_{n \in N} fol_n^b; \quad \forall n \in N \tag{14}$$

### 4.4 Ultracapacitor

The ultracapacitor is defined similarly to the battery, including equations for the evolution of the state of charge in each cycle, its limits and the maximum power. The main difference with the battery is the necessity of operating with a DC/DC converter, which affects both the maximum power and the cost. The cost of the converter has been included in a single cost with the cost of the ultracapacitors ($C^u$).

The DC/DC converter affects to the efficiency of storing energy in ultracapacitors. This efficiency is included in the efficiency value of the ultracapacitors ($\eta^{u,c}$) in the equation of the state of charge ($soc_n^u$) at the end of each cycle (15).

$$soc_n^u = soc_{n-1}^u + (\eta^{inv} \cdot \eta^{u,c} \cdot e_n^{u,c} - \frac{e_n^{u,d}}{\eta^{inv} \cdot \eta^{u,d}}); \forall n \in N \tag{15}$$

$$soc_0^u = 0 \tag{16}$$

Moreover, although the ultracapacitors can be completely discharged, the DC/DC converter provides a minimum state of charge ($\underline{SOC}^u$) restriction that is related to the working voltage. The equations (17) and (18) include both this constraint and the upper limit state of charge, which corresponds to the maximum capacity of the ultracapacitor.

$$e_{rated}^u \geq soc_n^u; \quad \forall n \in N \tag{17}$$

$$\underline{SOC}^u \cdot e_{rated}^u \leq soc_n^u; \quad \forall n \in N \tag{18}$$

The maximum $C-Rate$ of the ultracapacitor and, therefor, the maximum power have been determined with (19) and (20) following the information provided in [19] in a conservative way.

$$\frac{e_n^{u,c}}{\Delta T_n} \leq Crate^{u,max} \cdot e_{rated}^u; \quad \forall n \in N \tag{19}$$

$$\frac{e_n^{u,c}}{\Delta T_n} \leq Crate^{u,max} \cdot e_{rated}^u; \quad \forall n \in N \tag{20}$$

### 4.5 Maximum profile power

In addition to the above equations, a restriction has been included to guarantee that both the battery and the ultracapacitor are capable of dealing with the operating profile at all times.

$$P^{max} \leq Crate^{b,max} \cdot e_{rated}^b + Crate^{u,max} \cdot e_{rated}^u; \tag{21}$$

### 4.6 Objective function

The objective function of the problem is defined in the equation (22), which seeks to minimize the operating cost of the studied profile taking into account the costs of the power converters, the battery, and the ultracapacitors, as well as the degradation of these components in the operation. In order to compute the operation cost of each component, the capital cost is multiplied by the fraction of life consumed. The fraction of life consumed by the battery is calculated in eq. (14), while that consumed by converters and ultracapacitors is based on their calendar life.

$$\min_{variables} \left\{ C^{inv} \cdot p^{inv} \cdot \frac{T^{prof}}{CL^{inv}} + C^b \cdot e_{rated}^b \cdot fol^b + \right. \\ \left. + C^u \cdot e_{rated}^u \cdot \frac{T^{prof}}{CL^u} \right\} \tag{22}$$

## 5 Case study

The proposed methodology allows to get the optimal size of a HESS taking into account the battery ageing by operation. The case studies in this section has been selected to show how the proposed method can be used to:

- On one hand, evaluate the more appropriate configuration for an energy storage system, single component or HESS, when battery ageing by operation is taken into account.
- On the other hand, to quantify the cost related to battery ageing by operation, for different applications, wind and PV, and different energy storage system configurations.

Four configurations are considered for the energy storage system:

A. Conventional battery.
B. High-end battery.
C. HESS: Conventional battery and ultracapacitor.
D. Ultracapacitor.

In configurations A and B, $e_{rated}^u$ is set to zero and the constrains related to the ultracapacitor are not taken into account, meanwhile in case D, $e_{rated}^b$ is set to zero, and the same happens with the battery constrains. For each configuration the system size and cost are computed in two cases:

i. Sizing and cost are calculated considering battery degradation by operation and calendar life.
ii. Sizing considering battery degradation only by calendar life, and cost is computed taking into account also the battery degradation by operation. In this case a "*" is added to the configuration name, for instance $A^*$.

All configurations use commercial components, their main features are listed on Table 1. Two kind of batteries are considered, a conventional battery and a high-end battery. The conventional battery corresponds to a mature technology and it is widely available. The high-end battery corresponds to a technology in development, it is available only on demand, and it has a cost much higher than this of the conventional battery. For the ultracapacitor: its C-rate is taken from [19], its cost includes the power electronics (DC/DC converter), the efficiency includes also the power electronics operation, and the lower bound for its state of charge is set by the lower bound for the operation of the DC/DC converter. The calendar life of the ultracapacitor is taken from a datasheet of a manufacturer [38].

Data for the conventional battery are taken from [31], its curve of cycles to failure is depicted in Fig. 3, the coefficients of this curve are listed on Table 1. The curve of cycles to failure of the high end battery is summarized on Table 2.

The resulting optimization problem is non-linear when battery degradation by operation is considered, and it is solved using CONOPT under GAMS. When only degradation by calendar life is considered, the resulting problem is linear and can be solved using CPLEX or CONOPT. The biggest problem considered in the case

**Table 1** Features of the system components

| | Conventional Battery | High-End Battery | UC | AC/AC |
|---|---|---|---|---|
| Cost ($/kW or kWh) | 500 | 3000 | 11000 | 150 |
| Efficiency (%) | 90 | 94 | 93 | 94 |
| C-rate max (-) | 3 | 5 | 80 | - |
| Lifespan (years) | 15 | 15 | 15 | 15 |
| Minimum SoC (%) | 20 | 5 | 20 | - |
| $\alpha$ (-) | 1.2 | 1.2 | - | - |
| $\beta$ (-) | 1.15 | 1.45 | - | - |
| $\gamma$ (-) | 4072 | 27045 | - | - |

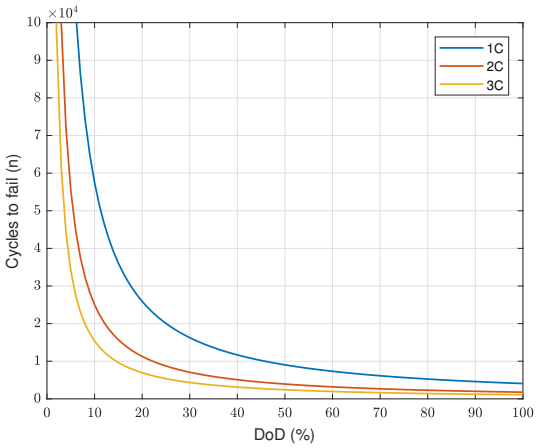


**Fig. 3**: Curves of cycles to failure for the conventional battery.

**Table 2** High end battery. Cycles to failure

| DoD (%) | 1C | 3C | 5C |
|---|---|---|---|
| 20 | 270000 | 74000 | 40000 |
| 50 | 73000 | 19000 | 10700 |
| 80 | 37000 | 10000 | 5400 |
| 100 | 27045 | 7200 | 3900 |

studies corresponds to an application involving wind generation during a whole day and battery degradation by operation. In that case it is a non-linear problem, the battery load profile contains around 800 cycles, and it takes around 25 seconds to be solved on a computer with Intel Core i5 7400 (4 cores @ 3 GHz) and 8 GB RAM.

As the problem is non-linear and non-convex there are not general results to assure if the global optimum has been reached or not. In our problem, the results provided correspond to local optima in the local domain where it makes sense for the variables to take values. Bounds for the variables in the problem have been estimated based on the problem physical interpretation and a linear problem without considering degradation has been used for this task. Several numerical tests have been performed to check that the reported solutions correspond to the optima inside those bounds (local domain).

Two groups of case studies are reported, one involving wind generation and the other involving photovoltaic generation, both groups are described and discussed in what follows.

### *5.1 Application Involving Wind Generation*

The application to wind generation is quite demanding, because the load profile can contain oscillations at any time of the day and of any magnitude in the range of the generator rated power. In this case study, a wind turbine with a rated capacity of 800 kW located in the Southern Spain is considered. Fig. 4 shows the power profile the storage has to face to smooth the wind turbine output. It should be noted the large number of power peaks during the whole day.

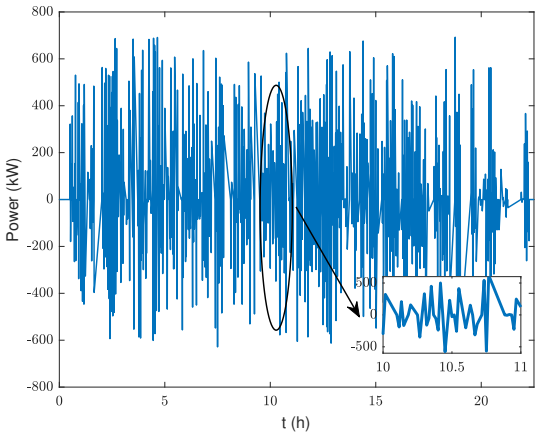


**Fig. 4**: Wind Case. Power profile

The proposed method is applied to the load profile depicted in Fig. 4 for different configurations of the storage system (A, B, C, D). Results considering degradation by operation are summarized in Table 3. These results are compared to those for the cases where sizing has been done considering only degradation by calendar life (A$^*$, B$^*$, C$^*$, D$^*$) in Table 4.

When degradation by operation is considered, battery degradation in each load cycle corresponds to the maximum value between: degradation by calendar life, and degradation by operation. Thus, only one of them is dominant in each cycle. To this regard, column "Op. %" in Table 3 stands for the percentage of the total battery degradation (for the whole load profile) in which the degradation by operation has been dominant.

**Table 3** Wind case. Results considering degradation by operation

| System | $e^b_{rated}$ (kWh) | $e^u_{rated}$ (kWh) | $Op.Cost$ ($/day) | $fol^b$ (-) | % Op |
|---|---|---|---|---|---|
| A (conv. bat.) | 692.64 | - | 109.14 | 2.60E-04 | 42.55 |
| B (high-end) | 207.64 | - | 173.55 | 2.48E-04 | 37.74 |
| C (HESS) | 123.18 | 11.4 | 59.61 | 2.88E-04 | 42.56 |
| D (ultra.) | - | 79.19 | 178.06 | - | - |

Regarding the results summarized in Table 3 it is interesting to highlight that:

- The HESS, (C), is the configuration with the lowest cost. And the difference is quite big, almost half the cost of the next best configuration. Configuration C allows to do the most of the best qualities of both components, battery to store energy (low C-rate and high storage) and ultracapacitor to provide power peaks (high C-rate and low storage). While in the single component configurations (A, B, D) some qualities of the component are underused.
- The constraint of energy storage (SoC) sets that capacity must be $\geq\approx 80$ kWh. This determines the ultracapacitor size $e^u_{rated} = 79.19$ kWh in D, that is also the configuration with the highest cost.
- The constraint of battery degradation by operation is active in all the configurations (except for the ultracapacitor, D), and it is the condition that determines the system size. The constraint for C-rate sets capacity $\geq 231$ kWh in configuration A, and $\geq 138.6$ kWh in configuration B, but the values on Table 3 are 692.64 kWh for configuration A, and 207.64 kWh for configuration B. Those values for configurations A and B are greater than the thresholds set by the SoC constraint (80 kWh) and C-rate constraint, 231 kWh for A, and 138.6 kWh for B. As only the constraint for the degradation by operation remains, that is what is determining the system size.

Table 4 shows the differences in component size when degradation by operation is taken into account (A, B, C) and when it is not

**Table 4** Wind case. Results considering (A, B, C) or not (A*, B*, C*) degradation due to operation

| Configuration | $e^b_{rated}$ (kWh) | $e^u_{rated}$ (kWh) | $Op.Cost$ ($/day) |
|---|---|---|---|
| A (conv. bat.) | 692.64 | - | 109.14 |
| A* (conv. bat.) | 231 | - | 231.00 |
| B (high-end) | 207.64 | - | 173.55 |
| B* (high-end) | 138.6 | - | 203.28 |
| C (HESS) | 123.18 | 11.4 | 59.61 |
| C* (HESS) | 230.29 | 0.03 | 221.80 |

(A*, B*, C*) to size the components. Operation cost on Table 4 is calculated considering degradation by operation and calendar life in all the cases: A, B, C, A*, B*, C*.

When only degradation by calendar life is considered to size the components (A*, B*, C*), the dominant constraint is that related to the component's C-rate. Thus the size is 231 kWh in A*, 138.6 kWh in B*, and 230.29 kWh of battery, 0.03 kWh of ultracapacitor in C*. Configurations A* and C* are very close, as the ultracapacitor size in C* is very small.

The most remarkable result illustrated on Table 4 is that disregarding degradation by operation in the sizing stage leads to operation costs much more higher than expected. For instance, in configuration A* costs are 110% higher than in A, in B* are 17% higher than in B, and in C*, the most interesting configuration, they are 270% higher than in C.

One can be tempted to disregard degradation by operation in the sizing stage, because it simplifies the calculation as it can be solved as a linear problem. But the error in the operation cost is not admissible, for instance in the case of the HESS it could be around 270%, as illustrated on Table 4.

It is expected a decrease in the battery cost in the next coming years, from the current 500 $/kWh to 200 $/kWh in ten years [8, 10, 11]. To illustrate how the relative size of components in configuration C (HESS) will change with the battery cost, a sensitivity analysis on that parameter has been performed, assuming the ultracapacitor cost remains constant. Results are depicted on Fig. 5, where we can observe a threshold for the battery cost, around 110 $/kWh. For a battery cost less than that threshold is not profitable to include the ultracapacitor in the system.

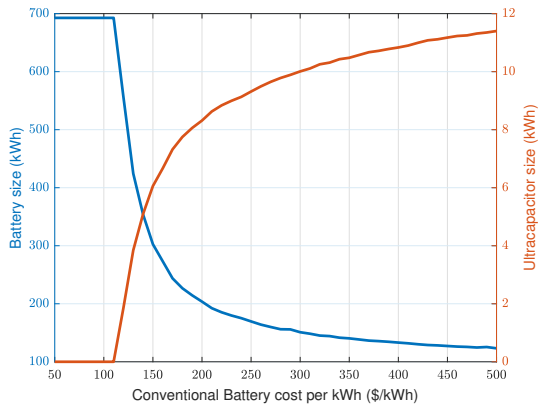


**Fig. 5**: Wind Case. Sensitivity analysis on battery cost for config. C.

### 5.2 *Application Involving PV Generation*

A real case study corresponding to a PV power plant of 500 kWp located near the equator is considered in this case study. A typical load profile faced by the storage system in this plant is depicted in

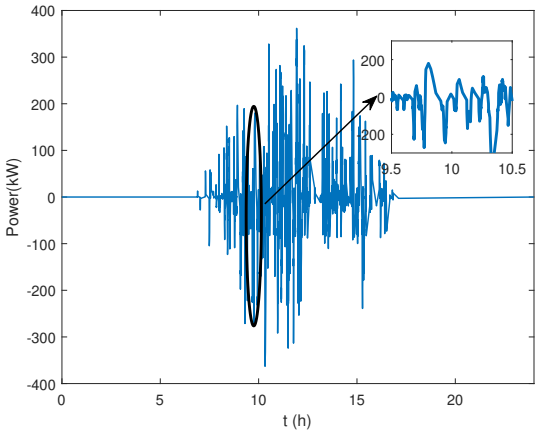


**Fig. 6**: PV case. Power profile

Fig.6. It is worth noting that the plant is operating around 10 hours, and the remaining 14 hours the load profile is flat with a zero value. That means the battery suffers degradation only by calendar life during 14 hours (58.3% of the day) and the remaining 10 hours it can suffer a combination of degradation by calendar life and operation. This makes the degradation by operation less relevant in this case than in the case with wind generation. Results are analogous to those for the wind application, but differences among configurations are smaller.

Results considering degradation by operation (A, B, C, D) are summarized on Table 5. Column $\%Op$ is interpreted as in Table 3, fraction of total degradation for which degradation by operation is dominant. As in the wind application, the lowest operation cost correspond to config. C (HESS), but the difference with config. A (only conventional battery) is very small. Results for A and C are determined by the constraint of degradation due to operation, result for B is set by the constraint related to C-rate, and result for D is determined by the constraint related to SoC.

**Table 5** PV case. Results considering degradation by operation

| System | $e^b_{rated}$ (kWh) | $e^u_{rated}$ (kWh) | $Op.Cost$ ($/day) | $fol^b$ (-) | % Op |
|---|---|---|---|---|---|
| A | 168.82 | - | 33.40 | 2.78E-04 | 42.96 |
| B | 72.58 | - | 59.21 | 2.26E-04 | 26.20 |
| C | 144.85 | 1.14 | 33.00 | 2.87E-04 | 42.94 |
| D | - | 52.30 | 115.02 | - | - |

**Table 6** PV case. Results considering (A, B, C) or not (A*, B*, C*) degradation due to operation

| System | $e^b_{rated}$ (kWh) | $e^u_{rated}$ (kWh) | $Op.Cost$ ($/day) |
|---|---|---|---|
| A (conv. bat.) | 168.82 | - | 33.40 |
| A* (conv. bat.) | 120.97 | - | 35.42 |
| B (high-end) | 72.58 | - | 59.21 |
| B* (high-end) | 72.58 | - | 59.21 |
| C (HESS) | 144.85 | 1.14 | 33.00 |
| C* (HESS) | 62.104 | 2.21 | 41.72 |

Results when only degradation by calendar life is considered (A*, B*, C*) are listed on Table 6, in this case the results for A*, B* and C* are determined by the constraint related to C-rate. In this case

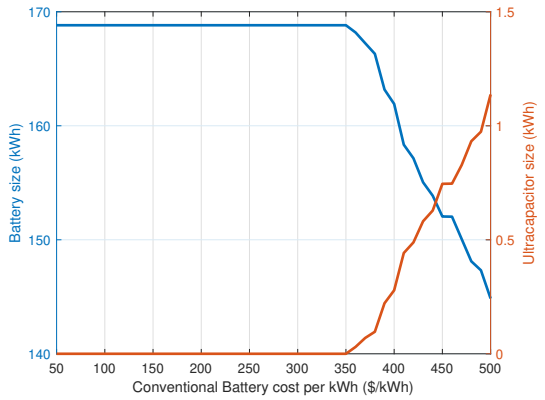


**Fig. 7**: PV Case. Sensitivity analysis on battery cost for config. C.

solutions when the constraint of degradation by operation are dominant and solutions when the constraint related to C-rate are dominant are similar. Thus, the error of disregarding degradation is smaller than in the case of wind generation. The error is around 6% for config. A, 26% for config. C and 0% for config. B, because B and B$^*$ are both determined by the constraint related to C-rate.

As in the wind case, a sensitivity analysis on the battery cost is performed for configuration C with PV generation. The results for the battery and ultracapacitor sizes are depicted in Fig. 7. It can be observed that for a battery cost $\leq$ 350 \$/kWh it is not profitable to include the ultracapacitor in the system, and for a battery cost $>$ 350 \$/kWh the change in the battery and ultracapacitor sizes is almost linear, that is because the degradation by calendar life (a linear constraint) is dominant over the degradation by operation (non-linear) during most of the load profile time.

In this case the threshold 350 \$/kWh is much higher than in the case of wind generation, 110 \$/kWh, that is because in this case the solutions considering degradation by operation are similar to those considering only degradation by calendar life. Thus the return from each monetary unit invested in the ultracapacitor is much lower in the case of the PV application than in the case of wind generation.

## 6 Conclusion

A methodology for sizing and operation of an hybrid electric (battery and ultracapacitors) energy storage system which explicitly takes into account battery degradation due to operation has been proposed.

The effectiveness of the algorithm has been illustrated in two case studies (wind and PV applications) showing that degradation is more relevant in the wind case since the operation profile shows continuous charging and discharging periods.

Several energy storage configurations have been analyzed. The hybrid configuration (battery and ultracapacitors) results in the lowest cost compared to non-hybrid solutions. This difference is larger in the wind case due to the greater variability of the source and the fact that photovoltaic energy does not generate throughout the night. The sizing of each component in the system depends on two main factors: i) the battery degradation by operation, which is related to the operation profile and the battery technology, and ii) the relative cost between battery and ultracapacitor; the more relevant the degradation by operation is, the greater relative cost of ultracapacitor can be assumed. The threshold for this relative cost has been quantified in both case studies.

Neglecting battery operation degradation effects can lead to greater operation cost and less battery life time than expected. Degradation by operation is quite relevant in the case of wind generation where the operation cost of the HESS (sized without considering degradation by operation) is 270% higher than the operation cost for the HESS considering degradation by operation. In the case of PV is less relevant, but still quite significant, as the HESS operation cost not considering degradation by operation is 26% higher than that of the HESS considering it.

## 7 Acknowledgments

This work has been partially funded by project ENE2016-80638-R granted by Ministerio de Economía y Competitividad of the Government of Spain.

## 8 References

1 Bloomberg New Energy Finance, "New Energy Outlook 2018," Tech. Rep., 2018. [Online]. Available: https://about.bnef.com/new-energy-outlook/
2 E. Rodrigues, R. Godina, S. Santos, A. Bizuayehu, J. Contreras, and J. Catalão, "Energy storage systems supporting increased penetration of renewables in islanded systems," *Energy*, vol. 75, pp. 265–280, 2014.
3 M. P. Musau, T. L. Chepkania, A. N. Odero, and C. W. Wekesa, "Effects of renewable energy on frequency stability: A proposed case study of the Kenyan grid," in *2017 IEEE PES PowerAfrica*. IEEE, 6 2017, pp. 12–15.
4 Puerto Rico Electric Power, "Minimum technical requirements for photovoltaic (PV) generation projects," 2012.
5 V. Gevorgian and S. Booth, "Review of PREPA Technical Requirements for Interconnecting Wind and Solar Generation," National Renewable Energy Laboratory, Tech. Rep., 2013.
6 A. Cabrera-Tobar, E. Bullich-Massagué, M. Aragüés-Peñalba, and O. Gomis-Bellmunt, "Review of advanced grid requirements for the integration of large scale photovoltaic power plants in the transmission system," *Renewable and Sustainable Energy Reviews*, vol. 62, pp. 971–987, 2016. [Online]. Available: http://dx.doi.org/10.1016/j.rser.2016.05.044
7 International Renewable Energy Agency, "Electricity Storage and Renewables: Cost and Markets to 2030," Tech. Rep., 2017.
8 I. Tsiropoulos, D. Tarvydas, and N. Lebedeva, "Li-ion batteries for mobility and stationary storage applications | EU Science Hub," Publications Office of the European Union, Tech. Rep., 2018.
9 L. Goldie-Scot, "A Behind the Scenes Take on Lithium-ion Battery Prices," *BloombergNEF*, 3 2019. [Online]. Available: https://about.bnef.com/blog/behind-scenes-take-lithium-ion-battery-prices/
10 International Renewable Energy Agency, "Electricity storage and renewables: Costs and markets to 2030," Tech. Rep., 2017. [Online]. Available: https://www.irena.org/publications/2017/Oct/Electricity-storage-and-renewables-costs-and-markets
11 O. Schmidt, A. Hawkes, A. Gambhir, and I. Staffell, "The future cost of electrical energy storage based on experience rates," *Nature Energy*, vol. 2, no. 8, p. 17110, 8 2017. [Online]. Available: http://www.nature.com/articles/nenergy2017110
12 F. Diaz-Gonzalez, F. D. Bianchi, A. Sumper, and O. Gomis-Bellmunt, "Control of a Flywheel Energy Storage System for Power Smoothing in Wind Power Plants," *IEEE Transactions on Energy Conversion*, vol. 29, no. 1, pp. 204–214, 3 2014.
13 A. Oudalov, R. Cherkaoui, and A. Beguin, "Sizing and Optimal Operation of Battery Energy Storage System for Peak Shaving Application," in *2007 IEEE Lausanne Power Tech*. IEEE, 7 2007, pp. 621–625.
14 Y. Yang, H. Li, A. Aichhorn, J. Zheng, and M. Greenleaf, "Sizing Strategy of Distributed Battery Storage System With High Penetration of Photovoltaic for Voltage Regulation and Peak Load Shaving," *IEEE Transactions on Smart Grid*, vol. 5, no. 2, pp. 982–991, 3 2014.
15 S. Canevese, A. Gatti, E. Micolano, L. Pellegrino, and M. Rapizza, "Battery Energy Storage Systems for frequency regulation: Simplified aging evaluation," in *2017 6th International Conference on Clean Electrical Power (ICCEP)*. IEEE, 6 2017, pp. 291–297.
16 Y. Liu, W. Du, L. Xiao, H. Wang, S. Bu, and J. Cao, "Sizing a Hybrid Energy Storage System for Maintaining Power Balance of an Isolated System With High Penetration of Wind Generation," *IEEE Transactions on Power Systems*, vol. 31, no. 4, pp. 3267–3275, 7 2016.
17 M. H. Nehrir, C. Wang, K. Strunz, H. Aki, R. Ramakumar, J. Bing, Z. Miao, and Z. Salameh, "A Review of Hybrid Renewable/Alternative Energy Systems for Electric Power Generation: Configurations, Control, and Applications," *IEEE Transactions on Sustainable Energy*, vol. 2, no. 4, pp. 392–403, 10 2011.
18 L. W. Chong, Y. W. Wong, R. Kumar Rajkumar, R. Kumar Rajkumar, and D. Isa, "Hybrid energy storage systems and control strategies for stand-alone renewable energy power systems," *Renewable and Sustainable Energy Reviews*, pp. 174–189, 2016.
19 Maxwell Technologies, "Grid storage application brief," pp. 20–21, 2012, http://www.maxwell.com/images/documents/maxwell_ultracapacitor_grid_storage_solutions.pdf, accessed on Mar 20, 2019.
20 A. Ostadi and M. Kazerani, "A Comparative Analysis of Optimal Sizing of Battery-Only, Ultracapacitor-Only, and Battery-Ultracapacitor Hybrid Energy Storage Systems for a City Bus," *IEEE Transactions on Vehicular Technology*, vol. 64, no. 10, pp. 4449–4460, 10 2015.
21 J. Snoussi, S. B. Elghali, M. Benbouzid, and M. F. Mimouni, "Optimal sizing of energy storage systems using frequency-separation-based energy management for fuel cell hybrid electric vehicles," *IEEE Transactions on Vehicular Technology*, vol. 67, no. 10, pp. 9337–9346, oct 2018.
22 G. Wang, M. Ciobotaru, and V. G. Agelidis, "Power Smoothing of Large Solar PV Plant Using Hybrid Energy Storage," *IEEE Transactions on Sustainable Energy*, vol. 5, no. 3, pp. 834–842, 7 2014.

23 D. Álvaro, R. Arranz, and J. A. Aguado, "Sizing and operation of hybrid energy storage systems to perform ramp-rate control in PV power plants," *International Journal of Electrical Power & Energy Systems*, vol. 107, pp. 589–596, 5 2019.

24 C. Ma, S. Dong, J. Lian, and X. Pang, "Multi-Objective Sizing of Hybrid Energy Storage System for Large-Scale Photovoltaic Power Generation System," *Sustainability*, vol. 11, no. 19, p. 5441, oct 2019. [Online]. Available: https://www.mdpi.com/2071-1050/11/19/5441

25 Ming Pang, Yikai Shi, W. Wang, and Xiaoqing Yuan, "A method for optimal sizing hybrid energy storage system for smoothing Fluctuations of Wind Power," in *2016 IEEE PES Asia-Pacific Power and Energy Engineering Conference (APPEEC)*. IEEE, 10 2016, pp. 2390–2393.

26 V. Knap, S. K. Chaudhary, D.-I. Stroe, M. Swierczynski, B.-I. Craciun, and R. Teodorescu, "Sizing of an Energy Storage System for Grid Inertial Response and Primary Frequency Reserve," *IEEE Transactions on Power Systems*, vol. 31, no. 5, pp. 3447–3456, 9 2016.

27 B. Xu, A. Oudalov, A. Ulbig, G. Andersson, and D. S. Kirschen, "Modeling of Lithium-Ion Battery Degradation for Cell Life Assessment," *IEEE Transactions on Smart Grid*, vol. 9, no. 2, pp. 1131–1140, 3 2018.

28 C. Liu, Y. Wang, and Z. Chen, "Degradation model and cycle life prediction for lithium-ion battery used in hybrid energy storage system," *Energy*, vol. 166, pp. 796–806, 1 2019.

29 J. Salpakari, T. Rasku, J. Lindgren, and P. D. Lund, "Flexibility of electric vehicles and space heating in net zero energy houses: an optimal control model with thermal dynamics and battery degradation," *Applied Energy*, vol. 190, pp. 800–812, mar 2017.

30 S. De la Torre, J. M. González-González, J. A. Aguado, and S. Martín, "Optimal Battery Sizing considering Degradation fo Renewable Energy Integration," *IET Renewable Power Generation*, 12 2018.

31 SAFT, "Lithium-Ion Battery Life. Solar photovoltaic (PV)-Energy Storage Systems (ESS)," Tech. Rep., 2014. [Online]. Available: www.saftbatteries.com

32 H. Yu and D. Cao, "Multi-objective Optimal Sizing and Real-time Control of Hybrid Energy Storage Systems for Electric Vehicles," in *IEEE Intelligent Vehicles Symposium, Proceedings*, vol. 2018-June. Institute of Electrical and Electronics Engineers Inc., oct 2018, pp. 191–196.

33 M. Pang, Y. Shi, W. Wang, and S. Pang, "Optimal sizing and control of hybrid energy storage system for wind power using hybrid Parallel PSO-GA algorithm," *Energy Exploration & Exploitation*, vol. 37, no. 1, pp. 558–578, jan 2019. [Online]. Available: http://journals.sagepub.com/doi/10.1177/0144598718784036

34 S. K. Kollimalla, M. K. Mishra, and N. L. Narasamma, "Design and analysis of novel control strategy for battery and supercapacitor storage system," *IEEE Transactions on Sustainable Energy*, vol. 5, no. 4, pp. 1137–1144, oct 2014.

35 J. Shen and A. Khaligh, "A supervisory energy management control strategy in a battery/ultracapacitor hybrid energy storage system," *IEEE Transactions on Transportation Electrification*, vol. 1, no. 3, pp. 223–231, oct 2015.

36 F. S. Garcia, A. A. Ferreira, and J. A. Pomilio, "Control strategy for battery-ultracapacitor hybrid energy storage system," in *Conference Proceedings - IEEE Applied Power Electronics Conference and Exposition - APEC*, 2009, pp. 826–832.

37 T. Zimmermann, P. Keil, M. Hofmann, M. F. Horsche, S. Pichlmaier, and A. Jossen, "Review of system topologies for hybrid electrical energy storage systems," *Journal of Energy Storage*, vol. 8, pp. 78–90, 11 2016.

38 Maxwell Technologies, "Datasheet: 240 V 3.75 F Ultracapacitor Module," 2018.